IEEE Access
Multidisciplinary | Rapid Review | Open Access Journal

Received 20 July 2022, accepted 28 July 2022, date of publication 5 August 2022, date of current version 10 August 2022.

Digital Object Identifier 10.1109/ACCESS.2022.3196773

RESEARCH ARTICLE

Multimodality for Reliable Single Image Based Face Morphing Attack Detection

RAGHAVENDRA RAMACHANDRA[1,2], (Senior Member, IEEE), AND GUOQIANG LI[2], (Member, IEEE)

[1]Institution of Information Security and Communication Technology (IIK), Norwegian University of Science and Technology (NTNU), 2815 Gjøvik, Norway
[2]MOBAI AS, 2821 Gjøvik, Norway

Corresponding author: Raghavendra Ramachandra (raghavendra.ramachandra@ntnu.no)

This work was supported by the European Union's Horizon 2020 Research and Innovation Program under Grant 883356.

ABSTRACT Face morphing attacks have demonstrated a high vulnerability on human observers and commercial off-the-shelf Face Recognition Systems (FRS), especially in the border control scenario. Therefore, detecting face morphing attacks is paramount to achieving a reliable and secure border control operation. This work presents a novel framework for the Single image-based Morphing Attack Detection (S-MAD) based on the multimodal regions such as eyes, nose, and mouth. Each of these regions is processed using colour scale-space representation on which two different types of features are extracted using Binarised Statistical Image Features (BSIF) and Local Binary Features (LBP) techniques. These features are then fed to the classifiers such as Probabilistic Collaborative Representation Classifier (P-CRC) and Spectral Regression Kernel Discriminant Analysis (SRKDA). Their decisions are combined at score level to make the final decision. Extensive experiments are carried out on three different face morphing datasets to benchmark the performance of the proposed method with the existing methods. Further, the proposed method is benchmarked on the Bologna Online Evaluation Platform (BOEP). Obtained results demonstrate the improved performance of the proposed method over existing state-of-the-art methods.

INDEX TERMS Biometrics, attacks, face biometrics, morphing attacks, multimodal modality.

I. INTRODUCTION

Face Recognition Systems (FRS) are widely deployed in security-based applications, including border control scenarios. Face biometrics is employed as the primary identifier to claim the subject's identity in electronic passports. The wide applicability of the face biometrics can be attributed to its easy enrollment process, user-friendly and easily verified by the human observer during passport issuance and border control. However, the evolving attacks on face biometrics have demonstrated the possibility of overriding the passport issuance protocols by introducing morphing attacks. Morphing is a process of blending one or more source images such that the resulting image will represent the salient characteristics of the source images [34]. Thus, the face morphing process will enable the attacker to generate a new face image similar to the face images used to create the morphing attack. Hence the generated face morphing image can be used to fool both human observers at passport issuance and FRS at the Automatic Border Control (ABC) gates [10], [16], [26], [34] resulting in high vulnerability. Further, the face morphing is demonstrated to be vulnerable even on infants [33]. Hence, the development of Morph Attack Detection (MAD) to automatically detect these attacks is of paramount importance.

The face MAD techniques available in the literature can be broadly divided into Single image-based MAD (S-MAD) and Differential image-based MAD (D-MAD) [34]. The S-MAD techniques use a single image, and D-MAD techniques will use two images to detect the morphing attacks. Among these two approaches, the single image-based morph detection is very challenging due to the variation in the face image quality, and this is further justified by the NIST FRVT MORPH [18] benchmark. Hence, in this work, we have focused on the problem of detecting the face morphing attack from a single face image.

The associate editor coordinating the review of this manuscript and approving it for publication was Vincenzo Conti.

The S-MAD techniques are widely addressed in the literature; the first S-MAD technique was introduced by Raghavendra *et al.* [23] based on the micro-texture based approach to quantify the morphing noises. Since then, several S-MAD techniques have been introduced that can be broadly classified as [34] (a) texture-based (b) morphing noise-based and (3) deep learning-based. The texture-based methods include the use of standard texture descriptors such as Binarised Statistical Image Features (BSIF), Local Binary Features (LBP), Image gradient, Local Phase Quantisation (LPQ), Histogram of oriented gradients (HOG), Scale- Invariant Features (SIFT) and Speed-up Robust Features (SURF). In most cases, these texture features are classified using Support Vector Machine (SVM). The residual noise-based approaches extract the morphing noise resulting from the image blending process. Several techniques are investigated that includes: Photo Response Non-Uniformity (PRNU) [9], Context Aggregated Network (CAN) [30] and colour denoising techniques [31]. The third type of S-MAD technique is based on deep learning techniques. Most of the deep learning techniques introduced in the literature are based on using the pre-trained CNN networks that can be attributed to the small face morphing dataset. To this extent, several pre-trained models are employed to perform the S-MAD. For a more detailed review on the state-of-the-art on S-MAD, readers are referred to the [34].

The recent works (after the publication of the survey article [34] on the S-MAD continued to use both hand-crafted features [3], [5] and the deep learning features [4], [8]. In [5] presents the scale-space features using 2D Discrete Wavelet Transform (2D-DWT) where discriminative wavelets are selected based on the entropy. The selected wavelet sub-bands are then classified using pre-trained Inception Resnet-v1 architecture. The results are presented on the small dataset with only 314 images in which 183 morphed and 131 bona fide face images. In [3] presented a technique based on the LBP features from which the discriminative features are selected using Neighbourhood Component Analysis (NCA) and classification using K-Nearest Neighbour (KNN), Decision Tree Classifier (DTC) and Naïve Bayes (NB) classifier independently. Experiments are presented on the small scale datasets with the improved sharpness as the post-processing. In [4] presents the attention-based deep CNN which uses Inception Resnet v1 as a backbone. Experiments are carried out by combining different morph generation schemes indicating the performance improvement over hand-crafted MAD methods. In [8], pixel-wise morphing attack detection (PW-MAD) solution is presented and experimented on small scale datasets to benchmark the generalisation. Thus, based on the available work, it can be noted that the existing deep CNN based methods can only use the pre-trained network due to the small scale of the database. However, the pre-trained networks are not robust enough to generalize on various variations (e.g. morphing generation type, post-processing, ageing, etc.) in the morphing image due to the limited availability of datasets. Hence, the hand-crafted features are still the favourite choice to improve the state-of-the-art performance.

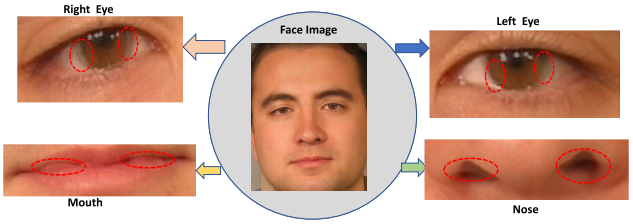

FIGURE 1. Artefacts due to morphing process (indicated in red dotted lines) illustration in the multimodal regions (eyes, mouth and nose) from face.

This work introduce a new framework based on multimodal features from the face to detect single image-based morphing attacks. The face region consists of four distinct regions: periocular (both left and right), nose, and mouth. The face morphing process will generate the artefacts in these salient regions of the face, and thus, using these regions independently will improve the morphing image detection accuracy. Figure 1 shows the multimodality from the face region in which the morphing artefacts are highlighted. These factors have motivated us to propose a new S-MAD technique based on multimodality from the face region. The major challenge in developing the S-MAD technique is the lack of availability of large-scale datasets. Therefore, the majority of the existing methods are based on hand-crafted features. Among the hand-crafted features, the scale-space features have indicated the best detection performance. Inspired by the robustness of the scale-space features, we designed the proposed method based on the scale-space features extracted using a Laplacian pyramid. Mainly, we extract the colour scale-space representation that is further processed using LBP and BSIF features independently and classified using a Probabilistic Collaborative Representation Classifier (P-CRC) and Spectral Regression Kernel Discriminant Analysis (SRKDA) classifiers. Finally, the comparison scores are combined using the weighted sum rule to make the final decision. The proposed scheme will run independently on the five salient regions, including face, left periocular, right periocular, nose and mouth to further explore the complementary features to improve the reliable morphing attack detection. In this work, we aim to seek answers to the following research questions, which will be answered systematically in this paper:

- **RQ#1:** Does the use of multimodality will improve the overall performance of S-MAD?
- **RQ#2:** Does the proposed S-MAD algorithm can indicate superior performance irrespective of the morphing generation techniques (e.g. landmark and deep learning-based)?
- **RQ#3:** Does the proposed method indicates improved performance on the morphing data with ageing?
- **RQ#4:** Does the manual post-processing to remove morphing artefacts in the morphed face image can degrade the performance of the proposed method?

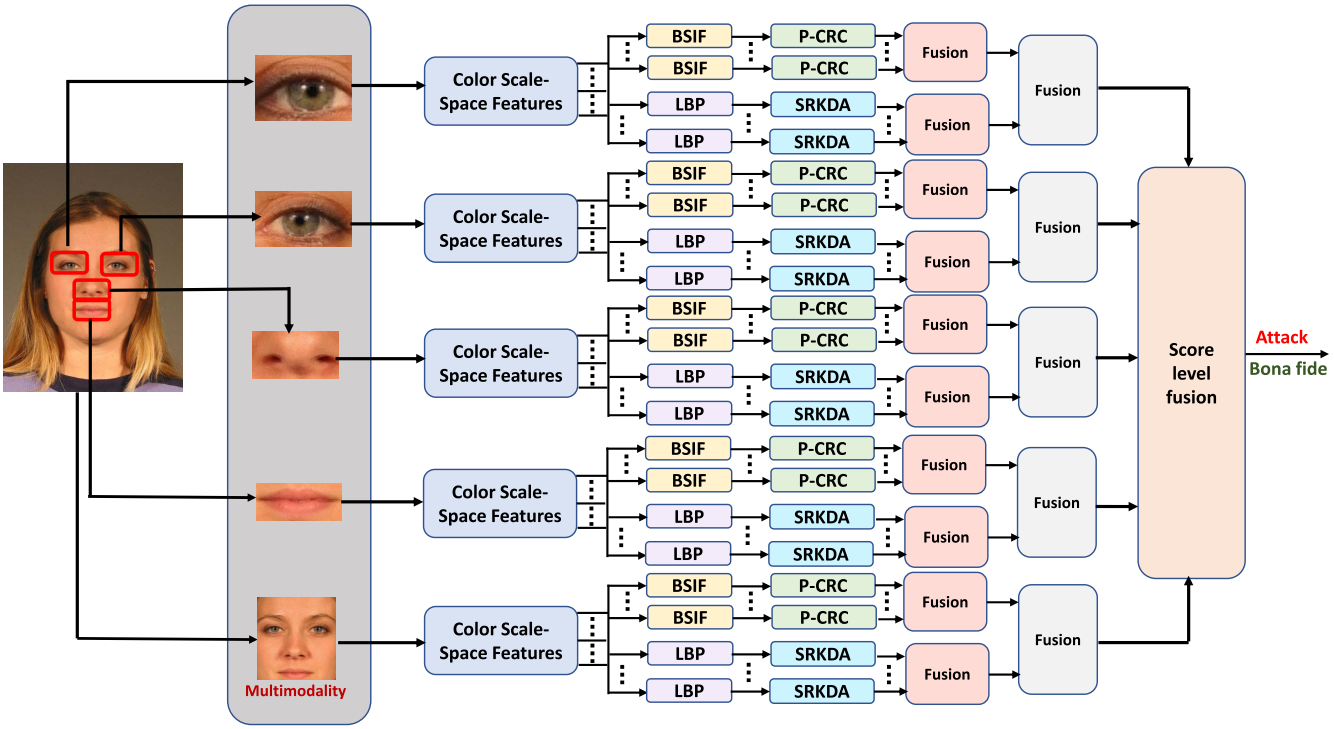

FIGURE 2. Block diagram of the proposed method.

- **RQ#5:** Does the proposed method can result in improved generalisability to an unknown source of morphing process when compared to existing methods?

In this work, we address the above presented research questions in a systematic manner through the following contributions:

- We present a novel S-MAD technique based on multimodality. To our knowledge, this is the first work that introduces multimodality for S-MAD detection. Further, we also present the colour scale-space based multi-feature technique to extract the discriminant features from the multimodal regions of the face that are combined at comparison score level to make the final decision.
- Extensive experiments are carried out on three different datasets to benchmark the detection performance of the proposed method with existing state-of-the-art methods. These three different databases are semi-publicly available for the research community.
- The proposed method is extensively evaluated to benchmark the generalizability to a different kind of morph generation method and the morphing source (e.g. digital and print-scan).
- The proposed method is extensively benchmarked to study the detection performance degradation on the effect of manual post-processing in both digital and print-scan mediums.
- The proposed method is benchmarked on the Bologna Online Evaluation Platform (BOEP).

The rest of the paper is organised as follows: Section II discuss the proposed method, Section III presents the quantitative results of the proposed method on three different datasets together with the state-of-the-art algorithms. Section V discuss the benchmark results on publicly available platform. Finally, Section VI draws the conclusion.

II. PROPOSED APPROACH

Figure 2 shows the block diagram of the proposed method to reliably detect the face morphing attacks using single image. *The novel part of the proposed method is the utility of multimodality achieved by independently processing the salient regions from the face to explore both complementarities and taking advantage of the morphing artefacts predominant in these regions.* Inspired by the success of the scale-space features [5], [25] in detecting the morphing attacks, in this work, we proposed a new framework using scale-space representation followed by the texture-based features with two different classifiers such as P-CRC and SRKDA. The proposed method consists of four functional blocks: multimodal region extraction, colour scale-space representation, feature representation, classification and multi-level fusion. In the following, we discuss each of these functional blocks in detail.

A. MULTIMODAL REGION EXTRACTION

The main objective of this step is to extract the salient regions from the face image effectively. The salient regions include the detected face, left periocular, right periocular, nose and mouth. Given the face image F_i, we have employed the Dlib

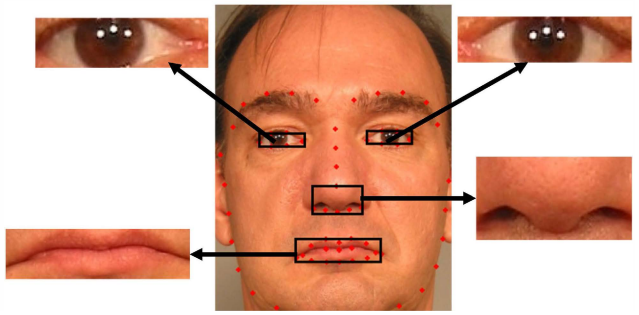

FIGURE 3. Illustration of extracting multi-modality using facial landmarks.

library[1] to extract the 68 different facial landmarks. These computed landmarks points include different facial regions such as chin and jawline, eyebrows, nose, eyes, and lips. Figure 3 illustrates the landmark detection using Dlib library and since the facial images are captured in the constrained conditions the landmark detection is reliable. The landmark detection will provide an estimate of 68 landmark points that are annotated with respect to the facial regions. For example, to segment the right eye, we have used the landmarks with annotation 43.44.45.46,47 and 48. We develop the rectangle starting from landmark annotated point 43 and we decide the width by counting pixels between annotated points 43 and 46 and the height is computed by counting the pixel between 45 and 47. Figure 3 illustrates the rectangle computed on the right eye. We followed the similar procedure with the left eye using the annotated landmarks 37 till 42 to compute the rectangle as shown in the Figure 3. For the nose region, we are interested in the frontal part as the morphing noises are more visible due to the geometric mismatch. To effectively extract the nose region, we have used the annotated landmark points 31 till 36. Figure 3 shows the rectangle segmentation region computed using these annotated landmarks. Lastly, we segment the mouth region by considering the outer landmarks annotated with 49-60 that are use to estimate the width and height of the rectangle as shown in the Figure 3. Thus, the extracted salient regions from the $F_i = FD_i, LP_i, RP_i, No_i \& Mo_i$ where FD_i represents the detected face region, LP_i represent the left periocular region, RP_i represent the right periocular region, No_i represent the nose region and Mo_i represents the mouth region. Figure 1 and 3 shows the qualitative results of the extracted salient regions from the face image.

B. COLOR SCALE-SPACE REPRESENTATION

Given the salient regions, we obtain the color scale-space representation independently for each region. Given the FD_i, the first step is to extract the color space. To this extent, we have used both YC_bC_r and HSV color channel based on their sensitivity to the morphing artefacts as demonstrated in [21], [31]. Thus, the color channel representation for FD_i be $FD_{Col} = FD_H, FD_S, FD_V, FD_Y, FD_{C_b}, FD_{C_r}$. In the next step, we extract the scale-space features independently on each of the color images using Laplacian pyramid [7]. In this work, we have selected the Laplacian pyramid over similar techniques such as steerable pyramids [14] or wavelets by considering its effective representation that can highlights the morphing artefacts. Given the color space image FD_H, we use three level decomposition that will result in the $FD_{H1}, FD_{H2}, FD_{H3}$. In this work, we have used six different color channels thus, the corresponding scale-space representation will result in $6 \times 3 = 18$ sub-images that are independently processed to extract the multiple features. Let the sub-images be represented as: $SI_k = SI_1, SI_2, \ldots, SI_{18}$, $\forall k = 1, 2, \ldots, 18$.

C. FEATURE REPRESENTATION AND CLASSIFICATION

Given the sub-image corresponding to the colour space representing the given salient region, we extract the micro-texture features using LBP and BSIF. The LBP reflects the correlation among pixels within a local area that quantifies the local information. In this work, we have extracted LBP features with a block size of 20×20 pixels with overlapping of 10 pixels and the neighbouring pixels as 8. This will result in a histogram features of size $2^8 = 256$ that in turn passed through the SRKDA classifier. The same sub-image is also used to extract the course texture features using a BSIF descriptor with a size of 17×17 and 12 bits, resulting in a feature vector of 4096. The BSIF features are further classified using the P-CRC classifier. In this work, we mainly employ the SRKDA for LBP features and P-CRC for BSIF features by considering the individual performance of the classifiers corresponding to individual features through the empirical study. We perform the feature extraction and classification independently on sub-images to obtain the corresponding comparison scores.

D. MULTILEVEL FUSION

This work presents a multi-level fusion approach to combine the comparison scores from sub-images corresponding to P-CRC and SRKDA classifiers. The first stage fusion is performed at the sub-image level between P-CRC and SRKDA classifiers scores that are computed independently on BSIF and LBP features. In this work, we have used the sum rule to perform the fusion of comparison scores. In the second level, the fusion scores from the first stage are combined using the sum rule between BSIF-PCRC and SRKDA. The fusion is carried out using the weighted sum rule between five different salient regions in the final stage. The weights are computed empirically [20] on the development dataset and kept constant throughout the testing. The computed weights are as follows: face = 0.25, left eye = 0.20, right eye = 0.20, nose = 0.20 and mouth = 0.15. These values are kept constant on all three datasets used in the experiments.

III. EXPERIMENTS AND RESULTS

In this section, we present extensive experiments to benchmark the performance of the proposed method on three different datasets. We first present the characteristics of three

[1] http://dlib.net

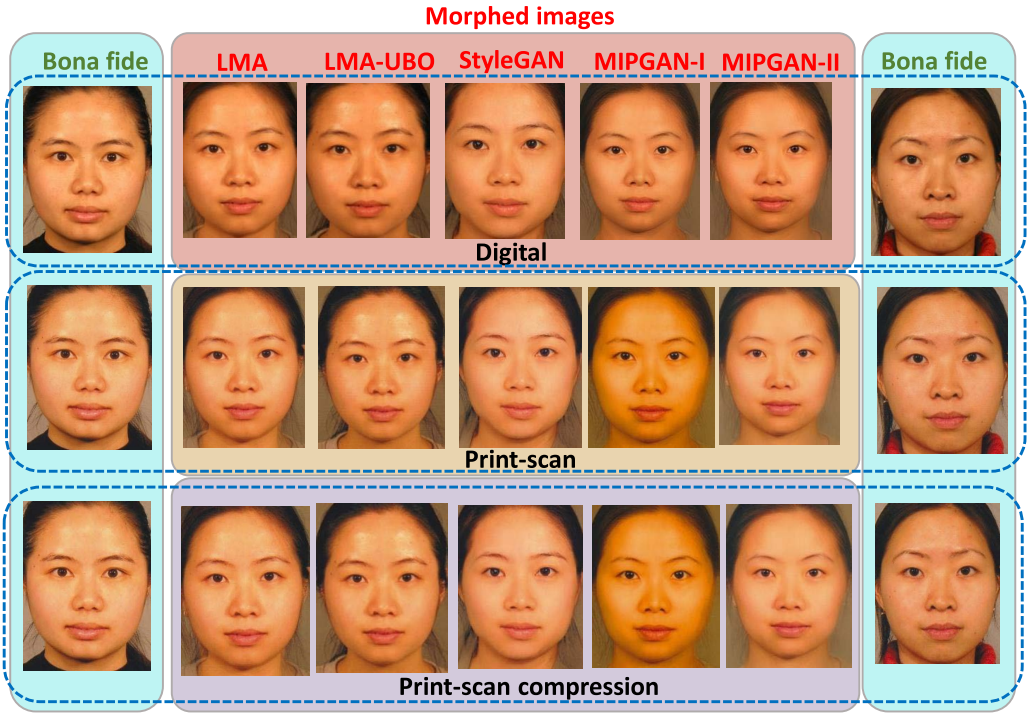

FIGURE 4. Example images from DB-I.

different datasets employed to benchmark the performance of the proposed method. We then present the quantitative results of the proposed method together with the existing methods. The quantitative performance of the MAD techniques is presented using the ISO/IEC metrics [15] namely the "Attack Presentation Classification Error Rate (APCER (%)) which defines the proportion of attack images (morph images) incorrectly classified as bona fide images and the Bona fide Presentation Classification Error Rate (BPCER (%)) in which bona fide images incorrectly classified as attack images are counted [15] along with the Detection Equal Error Rate (D-EER (%))" [36].

A. FACE MORPHING DATASETS

This section presents the characteristics of the three different datasets used to benchmark the quantitative performance of the proposed method. Each of these datasets is selected by considering the unique features that can cover the unique aspects such as the different morph generation, different print-scan processes, ageing and manual post-processing. All three databases are semi-publicly (researchers can submit the algorithms and get the benchmarked results or researchers can personally visit the authors institute to get complete access to the datasets) available for the research purpose. In the following, we describe the unique characteristics of these datasets.

1) DATABASE-I (DB-I)

DB-I dataset consists five different morph generation methods that include both landmarks and deep learning-based. DB-I was first introduced in [36] and generated from FRGC-V2 face database [19] to achieve high quality morphing images. DB-I consists of 140 data subjects, among which 47 are female, and 93 are male data subjects. The face morphing is generated using two different landmarks-based methods (Open CV [2] approach (referred as Landmark-I), and UBO [13] approach (referred as Landmark-II) with post-processing) and three different deep learning-based methods (MIPGAN-I, MIPGAN-II and StyleGAN). Further, DB-I consists of three different mediums such as digital, print-scan and print-scan with compression. The morphing is carried out by following the guidelines outlined earlier [21], [27], i.e., careful selection of subjects based on gender and comparison score using FRS to make attacks realistic. The DB-I consists of 2500×3 (types of morph data) $\times$ 4 types of morph generation technique $= 30,000$ morph samples and 1270×3 (types of morph data) $\times$ 4 types of morph generation technique $= 15,240$ bona fide samples [36]. Figure 4 shows the example images from the DB-I for the digital medium.

2) DATABASE-II (DB-II)

DB-II dataset is generated using landmark-based morph generation technique that is publicly available from OpenCV [2]. The unique characteristic of this dataset is the manual post-processing of the morphed face images to weed out the noise resulting from the morphing process. DB-II is constructed using the FRGC face dataset [19] from which 147 unique data subjects are selected by considering the enrolment quality. The morphing dataset is generated by

FIGURE 5. Example face image before and after post-processing.

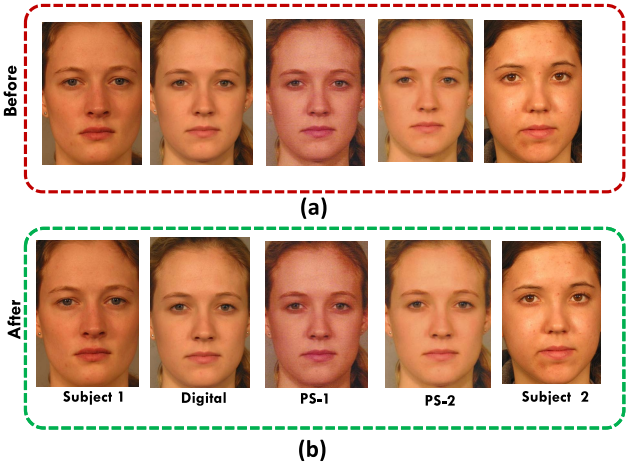

FIGURE 6. Example face images from DB-II: (a) before (b) after post-processing.

following the good practices discussed in [21], [27]. The generated morphing images are further processed manually using Adobe Photoshop to correct the errors resulting due to the morphing process. Figure 5 shows the example face image before and after post-processing, and it can be noted that the post-processing operation has resulted in high quality morphed images that are free from the morphing noises. DB-II consists of both digital and print-scan (with two different printers) data for both with and without post-processing. The DB-II consists of 1272 $\times$ 3 (types of medium) = 3816 bona fide and 1071 $\times$ 3 (types of medium) = 3213 morphed images. Figure 6 shows the example images from DB-II.

3) DATABASE-III (DB-III)

DB-III dataset is introduced in [32] and based on the MORPH II non-commercial dataset [6] and the unique characteristic of this dataset is the variation in age. DB-III has two age bins (1) MorphAge-I: This dataset consists of 1002 unique data subjects with an age variation of 1-2 years. This dataset has 10538 images (2) MorphAge-2: This dataset consists of 516 unique data subjects with an age variation of 2 to 5 years. This dataset has in total of 3767 images. Both of these datasets have used UBO face Morpher [13] to generate the morphed

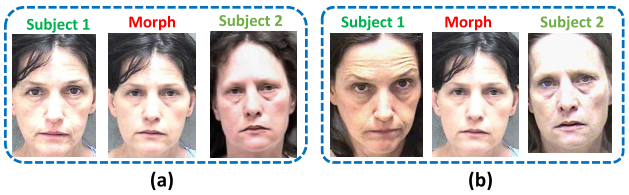

FIGURE 7. Example face image from MorphAge-I: (a) example at year=0 (b) example at year=1 to 2.

FIGURE 8. Example face image from MorphAge-II: (a) example at year=0 (b)example at year=2 to 5.

face images. Figure 7 and 8 shows the example images from DB-III.

B. RESULTS AND DISCUSSION ON DB-I

This section discusses the proposed method's quantitative results together with the state-of-the-art S-MAD techniques on the DB-I. The DB-I includes 690 bona fide images and 1190 morphed images in the training set and 580 bona fide and 1310 morphed images in the testing set. We design the experimental protocols to reflect the role of different morph generation techniques on the detection performance of the S-MAD techniques. To this extent, we have proposed both inter and intra experiment protocols. In the case of intra evaluation protocol, we train and test S-MAD techniques with the same type of morph generation technique. In contrast, inter evaluation protocol will use one type of morph generation technique for training and the rest of the morph generation technique for testing. Table 1, 2, 3, 4 and 5 shows the quantitative performance of the proposed method together with four recent state-of-the-art techniques from Deep features [22], Steerable features [24], [25] and [29]. We particularly choose these S-MAD techniques as these techniques have been widely evaluated on several types of morph generation techniques and different morph generation mediums and both of these techniques have indicated the best detection performance [36]. It is also worth noting that the Hybrid features [25] are benchmarked in the NIST FRVT MORPH challenge [18] indicating one of the top performances. These factors justify the selection of SOTA for comparison with the proposed method.

Based on the quantitative results obtained from the intra-dataset experiments, the following are the important observations:

- The intra evaluation protocol has indicated the high success rate in detecting the morphing attacks using both SOTA and the proposed method.

TABLE 1. Quantitative performance of the proposed method - Training- Landmarks-I [21].

Morph Generation Type: Training	Morph Generation Type: Testing	MAD Algorithms	Digital			Print-Scan			Print-scan Compression		
			D-EER(%)	BPCER@APCER		D-EER(%)	BPCER@APCER		D-EER(%)	BPCER@APCER	
				5	10		5	10		5	10
LMA	LMA	Ensemble features [29]	**0**	**0**	0	2.35	1.45	0.96	2.58	1.71	1.54
		Hybrid features [25]	0.16	0	0	1.85	0.85	0.34	2.25	1.12	0.51
		Deep features [22]	**0**	**0**	**0**	2.85	1.25	0.17	2.05	1.02	0.17
		Steerable features [24]	5.48	6.12	3.60	23.59	62.90	46.48	27.14	71.52	57.28
		Proposed Method	**0**	**0**	**0**	**0**	**0**	**0**	**1.42**	**0.71**	**0.17**
	LMA-UBO	Ensemble features [29]	49.55	92.22	88.85	41.93	81.45	76.25	42.15	83.88	77.64
		Hybrid features [25]	49.16	99.31	97.59	44.17	86.48	80.24	46.49	88.38	81.95
		Deep features [22]	42.36	88.46	77.28	41.90	85.04	72.30	41.58	91.17	71.11
		Steerable features [24]	64.20	99.48	98.45	50	93.89	88.13	47.39	92.14	83.68
		Proposed Method	**41.51**	**80.61**	**71.86**	**35.37**	**79.64**	**73.92**	**37.86**	**84.46**	**76.96**
	MIPGAN-I	Ensemble features [29]	39.16	73.12	65.35	9.45	14.57	8.74	8.95	15.26	9.26
		Hybrid features [25]	46.82	86.62	81.64	12.32	19.72	13.2	9.74	15.95	8.91
		Deep features [22]	44.94	84.59	74.47	3.73	2.40	1.02	23.83	66.55	49.22
		Steerable features [24]	50	99.82	97.59	3.26	2.22	2.15	28.82	79.24	60.20
		Proposed Method	**41.39**	**78.79**	**72.55**	**0**	**0**	**0**	**8.14**	**10.89**	**7.14**
	MIPGAN-II	Ensemble features [29]	34.13	70.49	61.57	5.32	6.68	2.57	6.72	8.16	4.14
		Hybrid features [25]	44.96	83.7	75.47	5.9	8.42	3.23	5.67	6.18	2.91
		Deep features [22]	40.37	60.32	50.36	1.36	0	0	8.37	24.69	16.17
		Steerable features [24]	50	98.77	97.25	6.84	7.54	6.12	31.16	85.42	73.75
		Proposed Method	**35.86**	**66.72**	**56.43**	**0**	**0**	**0**	**4.47**	**3.57**	**0.35**
	StyleGAN	Ensemble features [29]	0.22	0	0	13.36	27.44	16.46	14.77	27.27	19.38
		Hybrid features [25]	0.16	0	0	44.96	83.7	75.47	9.44	14.57	9.14
		Deep features [22]	0.16	0	0	1.08	0.17	0	8.92	12	8.17
		Steerable features [24]	7.16	9.77	4.63	3.46	2.42	1.54	38.91	87.30	79.58
		Proposed Method	**0**	**0**	**0**	**0**	**0**	**0**	**5.34**	**5.35**	**3.21**

- Among three different mediums (digital, print-scan and print-scan with compression), the S-MAD techniques has indicated outstanding performance on digital medium. In contrast, the performance is degraded with print-scan and print-scan with compression.
- The proposed method has indicated the best performance compared with two different state-of-the-art techniques.
- The proposed method has shown outstanding performance with D-EER $= 0\%$ on all different types of morphing generation techniques, especially with the digital medium. These results indicate the efficacy of the proposed method.
- The proposed method also indicates the best results compared to the SOTA on both print-scan and print-scan with compression. These results further justify the scalability of the proposed approach to the different mediums.

Based on the obtained results from the inter evaluation protocols, the following are the main observations:

- In general, the performance of the S-MAD algorithms are degraded in the inter evaluation protocol. However, the proposed method has indicated less degradation in the detection performance compared with the SOTA.
- Based on the obtained results, the morph generation technique used for training can impact the detection performance when tested with the other morphing generation techniques. This can be attributed to the nature of morphing generation techniques, and the post-processing applied after the generation of the morphed face image.
- The proposed method has indicated the best performance compared to the SOTA on most of the experiments. In some cases, the proposed method's degraded performance is noted only with the digital medium.
- The proposed method has shown outstanding performance on the print-scan medium. This can be attributed to the nature of the data, as the print-scan process with the same printer and scanner will somehow normalise the effect of morph generation techniques. Further, it can also be noted that the proposed method has indicated the best detection performance compared to SOTA on print-scan compression process data. Further, it can also be noted that the compression noise will degrade the performance of the proposed method compared to without compression, especially in the inter evaluation protocols.
- All-in-all, the proposed method has indicated the best performance in the inter evaluation protocol compared to the SOTA.

C. RESULTS AND DISCUSSION ON DB-II

This section presents the quantitative results on the DB-II to understand the role of manual post-processing in detection

TABLE 2. Quantitative performance of the proposed method - Training- Landmarks-II [13].

Morph Generation Type: Training	Morph Generation Type: Testing	MAD Algorithms	Digital			Print-Scan			Print-scan Compression		
			D-EER(%)	BPCER@APCER		D-EER(%)	BPCER@APCER		D-EER(%)	BPCER@APCER	
				5	10		5	10		5	10
LMA-UBO	LMA	Ensemble features [29]	48.57	97.77	95.36	**24.19**	**52.48**	**43.22**	**21.64**	**47.51**	**36.19**
		Hybrid features [25]	45.67	96.91	94.16	32.26	77.87	66.55	24.51	50.94	40.65
		Deep features [22]	47.22	89.94	68.98	26.66	55.40	42.53	25.24	51.80	40.99
		Steerable features [24]	50	95.12	91.25	37.72	93.48	82.84	37.13	92.62	83.71
		Proposed Method	**19.54**	**42.36**	**31.21**	34.29	84.28	72.32	38.19	81.42	71.25
	LMA-UBO	Ensemble features [29]	3.62	2.22	0.68	6.32	7.97	2.42	5.57	6.41	2.42
		Hybrid features [25]	1.53	0.17	0	5.21	5.19	3.14	5.37	5.71	3.46
		Deep features [22]	6.16	6.51	3.94	6.65	9.94	4.88	7.13	12.50	5.55
		Steerable features [24]	27.78	69.46	53.68	30.55	79.75	68.05	29.54	76.41	63.19
		Proposed Method	**0**	**0**	**0**	**1.61**	**0.53**	**0.35**	**1.82**	**0.35**	**0.17**
	MIPGAN-I	Ensemble features [29]	30.23	65.35	53.17	43.92	87.65	79.24	44.24	89.23	82.33
		Hybrid features [25]	46.29	84.04	77.01	34.16	71.18	64.66	35.5	76.84	65.52
		Deep features [22]	38.18	77.53	67.92	1.20	0.34	0.17	**27.41**	**65.69**	**52.65**
		Steerable features [24]	36.51	86.96	76.51	2.61	0.85	0	32.73	87.13	74.19
		Proposed Method	**24.75**	**52.14**	**42.88**	**0.37**	**0**	**0**	40.51	82.14	73.92
	MIPGAN-II	Ensemble features [29]	27.13	58.83	45.45	33.57	77.35	65.52	40.46	84.9	75.47
		Hybrid features [25]	46.82	83.53	75.81	35.91	77.18	65.24	36.5	79.24	68.78
		Deep features [22]	36.71	78.73	68.61	1.04	0	0	34.40	71.18	59.69
		Steerable features [24]	36.87	90.33	79.41	3.19	1.88	0.34	34.12	89.19	78.91
		Proposed Method	**20.92**	**33.27**	**43.05**	**0.91**	**0**	**0**	**33.33**	**77.85**	**67.5**
	StyleGAN	Ensemble features [29]	29.67	61.92	52.48	27.18	61.57	58.14	23.17	49.22	38.25
		Hybrid features [25]	34.76	74.44	62.95	34.8	67.23	79.24	44.24	89.23	82.33
		Deep features [22]	30.13	35.19	40.29	1.37	0,17	0.17	26.65	57.10	46.31
		Steerable features [24]	50	98.28	96.56	1.21	0.34	0	35.52	85.31	71.69
		Proposed Method	**25.4**	**62.09**	**49.91**	**0.16**	**0**	**0**	**15.53**	**31.96**	**23.21**

TABLE 3. Quantitative performance of the proposed method - Training- MIPGAN-I [36].

Morph Generation Type: Training	Morph Generation Type: Testing	MAD Algorithms	Digital			Print-Scan			Print-scan Compression		
			D-EER(%)	BPCER@APCER		D-EER(%)	BPCER@APCER		D-EER(%)	BPCER@APCER	
				5	10		5	10		5	10
MIPGAN-I	LMA	Ensemble features [29]	23.66	51.45	39.96	**5.82**	**7.22**	**2.92**	**6.17**	**7.54**	**3.94**
		Hybrid features [25]	47.15	87.16	79.41	6.5	8.23	4.15	7.91	10.29	6.34
		Deep features [22]	**11.63**	**23.11**	**12.56**	19.91	34.10	31.38	18.66	37.75	28.64
		Steerable features [24]	50	91.25	85.92	35.86	80.44	70.66	38.60	84.73	74.99
		Proposed Method	32.43	73.17	61.92	9.65	15.71	8.75	5.01	5	3.14
	LMA-UBO	Ensemble features [29]	35.38	82.33	68.95	41.67	95.14	83.53	43.68	96.01	85.44
		Hybrid features [25]	28.62	75.64	61.4	44.38	95.66	85.78	38.18	90.46	78.16
		Deep features [22]	38.40	89.02	77.70	45.21	86.17	80.27	42.80	96.50	90.48
		Steerable features [24]	50	97.94	93.82	44.36	87.26	81.15	43.92	92.36	86.55
		Proposed Method	**17.14**	**49.39**	**26.41**	**28.8**	**87.14**	**58.92**	**29.65**	**88.21**	**67.5**
	MIPGAN-I	Ensemble features [29]	**0**	**0**	**0**	**0**	**0**	**0**	**0**	**0**	**0**
		Hybrid features [25]	**0**	**0**	**0**	**0**	**0**	**0**	**0**	**0**	**0**
		Deep features [22]	1.16	0	0	**0**	**0**	**0**	**0**	**0**	**0**
		Steerable features [24]	29.83	84.21	68.95	0	0	0	25.92	72.72	60.14
		Proposed Method	**0**	**0**	**0**	**0**	**0**	**0**	**0**	**0**	**0**
	MIPGAN-II	Ensemble features [29]	2.15	0.17	0	0.68	0	0	0.64	0	0
		Hybrid features [25]	1.36	0.34	0	0.86	0	0	0.84	0	0
		Deep features [22]	2.01	1.02	0.34	0	0	0	0	0	0
		Steerable features [24]	34.56	88.16	78.38	0	0	0	28.58	85.93	69.12
		Proposed Method	**0**	**0**	**0**	**0**	**0**	**0**	**0**	**0**	**0**
	StyleGAN	Ensemble features [29]	**17.72**	**37.22**	**26.58**	12.19	26.24	15.26	11.82	24.69	14.23
		Hybrid features [25]	31.16	64.32	53.85	11.99	19.2	13.72	9.93	18.15	9.94
		Deep features [22]	26.86	27.54	24.63	0	0	0	10.46	8.74	6.43
		Steerable features [24]	50	92.45	87.15	0	0	0	44.12	92.45	86.79
		Proposed Method	22.81	48.37	37.22	**0**	**0**	**0**	**5.34**	**5.53**	**4.15**

accuracy. We have devised four different experiments to this extent: (1) Experiment-1: train and test S-MAD techniques on before post-process data. (2) Experiment-2: train and test S-MAD techniques after post-process (3) Experiment-3: train after and test before post-process data (4) Experiment-4: train before and test after post-process data. The DB-II includes

TABLE 4. Quantitative performance of the proposed method - Training- MIPGAN-II [36].

Morph Generation Type: Training	Morph Generation Type: Testing	MAD Algorithms	Digital			Print-Scan			Print-scan Compression		
			D-EER(%)	BPCER@APCER		D-EER(%)	BPCER@APCER		D-EER(%)	BPCER@APCER	
				5	10		5	10		5	10
MIPGAN-II	LMA	Ensemble features [29]	**13.08**	**29.15**	**15.78**	**4.28**	**3.94**	**2.22**	4.28	3.61	2.22
		Hybrid features [25]	40.14	77.7	67.23	5.49	5.48	2.4	7.21	10.98	4.15
		Deep features [22]	16.31	39.96	26.17	18.66	37.73	28.64	8.17	13.89	6.68
		Steerable features [24]	50	91.25	86.27	35.86	80.44	70.66	39.09	89.87	79.75
		Proposed Method	23.82	54.2	37.9	6.18	8.21	3.21	**4.16**	**3.39**	**1.96**
	LMA-UBO	Ensemble features [29]	32.37	84.9	70.32	40.22	88.9	79.2	38.96	94.28	82.14
		Hybrid features [25]	23.88	63.8	45.62	**13.72**	**29.67**	**18.18**	**14.25**	**31.73**	**20.41**
		Deep features [22]	41.10	90.92	83.87	42.807	96.50	90.40	35.12	76.56	70.13
		Steerable features [24]	48.94	97.77	92.79	44.36	87.26	81.15	45.47	92.53	88.71
		Proposed Method	**10.62**	**28.81**	**11.32**	26.8	82.32	64.28	30.15	90.53	73.21
	MIPGAN-I	Ensemble features [29]	1.56	0.68	0.34	2.14	1.22	0.53	**2.57**	**0.85**	**0.34**
		Hybrid features [25]	2.27	0.85	0.17	4.79	4.8	3.43	4.3	3.6	2.22
		Deep features [22]	2.41	0.55	0.17	0	0	0	7.85	10.97	5.31
		Steerable features [24]	30.51	83.70	69.29	0	0	0	26.24	82.33	62.63
		Proposed Method	**0**	**0**	**0**	**0**	**0**	**0**	3.89	2.85	1.78
	MIPGAN-II	Ensemble features [29]	**0**	**0**	**0**	**0**	**0**	**0**	**0**	**0**	**0**
		Hybrid features [25]	**0**	**0**	**0**	**0**	**0**	**0**	**0**	**0**	**0**
		Deep features [22]	2.57	1.02	0.51	**0**	**0**	**0**	3.58	1.2	0
		Steerable features [24]	31.84	86.79	70.84	**0**	**0**	**0**	26.57	85.59	72.21
		Proposed Method	**0**	**0**	**0**	**0**	**0**	**0**	**0**	**0**	**0**
	StyleGAN	Ensemble features [29]	**12.51**	**22.29**	**15.78**	13.72	29.67	18.18	14.25	31.73	20.41
		Hybrid features [25]	24.7	49.74	41.85	12.87	26.58	14.75	11.86	26.92	15.09
		Deep features [22]	21.70	33.49	23.72	**0**	**0**	**0**	7.18	9.43	4.45
		Steerable features [24]	50	95.19	92.45	**0**	**0**	**0**	46.30	91.54	90.56
		Proposed Method	21.15	40.48	30.87	**0**	**0**	**0**	**6.79**	**9.28**	**3.92**

TABLE 5. Quantitative performance of the proposed method - Training- StyleGAN [35].

Morph Generation Type: Training	Morph Generation Type: Testing	MAD Algorithms	Digital			Print-Scan			Print-scan Compression		
			D-EER(%)	BPCER@APCER		D-EER(%)	BPCER@APCER		D-EER(%)	BPCER@APCER	
				5	10		5	10		5	10
StyleGAN	LMA	Ensemble features [29]	0.32	0	0	16.6	28.13	19.89	13.89	22.12	17.66
		Hybrid features [25]	0.42	0	0	**15.26**	**26.41**	**17.66**	14.37	22.81	16.92
		Deep features [22]	0.16	0	0	24.67	55.74	41.80	13.36	34.30	18.69
		Steerable features [24]	6.17	7.71	3.94	33.92	81.81	69.46	35.62	83.87	74.19
		Proposed Method	**0**	**0**	**0**	20	41.96	29.64	**11.97**	**17.85**	**12.85**
	LMA-UBO	Ensemble features [29]	44.72	89.53	80.61	38.31	78.5	69.15	38.84	83.7	74.17
		Hybrid features [25]	45.65	90.22	84.56	34.18	81.95	70.53	32.93	78.5	64.12
		Deep features [22]	43.43	95.31	83.12	45.34	96.10	88.48	30.19	65.45	54.68
		Steerable features [24]	50	99.65	99.10	40.81	83.42	72.60	39.13	84.89	74.82
		Proposed Method	**42.69**	**88.5**	**78.38**	**26.72**	**73.21**	**56.25**	**27.87**	**68.75**	**57.14**
	MIPGAN-I	Ensemble features [29]	39.97	75.98	68.78	20.21	42.14	33.44	20.73	45.28	36.53
		Hybrid features [25]	46.45	86.79	77.87	29.34	59.19	47.51	24.87	51.62	41.18
		Deep features [22]	23.95	48.19	38.25	0	0	0	26.40	63.97	44.57
		Steerable features [24]	59.17	98.45	96.91	0	0	0	31.76	82.33	69.46
		Proposed Method	**33.73**	**69.53**	**61.69**	**0**	**0**	**0**	**20.07**	**39.46**	**30.39**
	MIPGAN-II	Ensemble features [29]	39.93	73.58	66.89	15.78	28.14	19.38	13.72	28.98	16.63
		Hybrid features [25]	44.72	82.16	73.75	19.36	43.22	28.64	16.98	32.93	23.84
		Deep features [22]	42.19	70.42	60.48	0	0	0	9.98	20.41	9.94
		Steerable features [24]	50	99.28	95.38	0	0	0	31.07	79.41	63.46
		Proposed Method	**37.56**	**75.98**	**65.86**	**0**	**0**	**0**	**7.85**	**12.67**	**5.17**
	StyleGAN	Ensemble features [29]	**0**	**0**	**0**	**0**	**0**	**0**	**0**	**0**	**0**
		Hybrid features [25]	**0**	**0**	**0**	**0**	**0**	**0**	**0**	**0**	**0**
		Deep features [22]	**0**	**0**	**0**	**0**	**0**	**0**	**0**	**0**	**0**
		Steerable features [24]	3.75	3.43	1.54	**0**	**0**	**0**	20.66	56.69	43.39
		Proposed Method	**0**	**0**	**0**	**0**	**0**	**0**	**0**	**0**	**0**

689 bona fide images and 517 morphed images in the training set, and 583 bona fide and 554 morphed images in the testing set. The detection performance of the proposed method is benchmarked against the existing S-MAD techniques such as Ensemble features [29], Deep features [22], Steerable features [24] and Hybrid features [25]. Table 6, 7, 8 and 9 indicates the quantitative results of the proposed method compared with the existing methods.

The following are the main observations based on the obtained results.

- The detection performance of the algorithms are influenced by the data medium. The digital medium generally indicates a better detection performance than the print-scan medium. Among the print-scan medium, the PS-I dataset is the most challenging one to detect, which can be attributed to the quality of the print-scan process.

TABLE 6. Quantitative performance of the proposed method on Experiment-1.

Training data	MAD algorithms	Testing Data								
		Digital			PS-I (canon)			PS-II (DNP)		
		D-EER(%)	BPCER@APCER		D-EER(%)	BPCER@APCER		D-EER(%)	BPCER@APCER	
			5%	10%		5%	10%		5%	10%
Digital	Ensemble features [29]	**0**	**0**	**0**	39.43	92.96	83.72	34.33	82.84	76.32
	Hybrid features [25]	**0**	**0**	**0**	41.16	89.19	79.24	39.98	87.65	77.35
	Deep features [22]	**0**	**0**	**0**	33.10	76.15	62.95	23.09	51.74	38.59
	Steerable features [24]	3.27	1.54	0.34	30.99	88.85	75.64	28.81	76.32	63.80
	Proposed Method	**0**	**0**	**0**	**30.14**	**75.88**	**61.45**	**24.14**	**76.15**	**63.12**
PS-I	Ensemble features [29]	17.48	238.93	27.95	6.14	7.37	4.13	10.1	17.15	10.46
	Hybrid features [25]	13.38	32.76	20.24	16.48	40.99	27.78	22.94	59.86	42.53
	Deep features [22]	20.27	43.15	32.93	5.63	6.68	3.25	14.10	29.67	19.72
	Steerable features [24]	21.27	64.67	47.68	14.36	41.68	23.34	30.36	86.62	76.15
	Proposed Method	**6.92**	**9.6**	**4.45**	**3.46**	**1.88**	**1.24**	**5.14**	**4.97**	**3.14**
PS-II	Ensemble features [29]	8.74	14.75	7.37	12.62	26.17	16.63	4.46	3.77	2.42
	Hybrid features [25]	8.19	11.49	7.54	8.56	11.66	7.14	1.91	0.85	0.17
	Deep features [22]	17.12	35.84	25.38	11.18	21.85	12.52	5.63	4.86	3.18
	Steerable features [24]	29.54	72.55	50.60	33.81	83.19	74.27	25.90	77.05	57.46
	Proposed Method	**4.64**	**4.11**	**2.22**	**24.76**	**58.83**	**47.34**	**12.23**	**25.72**	**15.26**

TABLE 7. Quantitative performance of the proposed method on Experiment-2.

Training data	MAD algorithms	Testing Data								
		Digital			PS-I (canon)			PS-II (DNP)		
		D-EER(%)	BPCER@APCER		D-EER(%)	BPCER@APCER		D-EER(%)	BPCER@APCER	
			5%	10%		5%	10%		5%	10%
Digital	Ensemble features [29]	**0**	**0**	**0**	50	97.77	93.99	38.45	87.82	79.58
	Hybrid features [25]	**0**	**0**	**0**	50	93.31	88.5	41.26	84.56	74.95
	Deep features [22]	**0**	**0**	**0**	42.68	82.14	69.79	30.78	59.57	47.56
	Steerable features [24]	3.54	1.54	0.68	47.77	94.27	79.17	39.69	89.19	75.81
	Proposed Method	**0**	**0**	**0**	**40.37**	**86.39**	**81.59**	**27.22**	**77.87**	**66.72**
PS-I	Ensemble features [29]	19.54	42.19	33.44	11.18	16.98	11.32	13.91	28.54	20.58
	Hybrid features [25]	13.36	26.75	17.49	17	50.77	35.67	23.18	58.31	45.79
	Deep features [22]	21.13	41.85	32.07	12.46	4.94	14.08	11.10	19.21	12.10
	Steerable features [24]	20.64	65.18	46.14	10.47	24.87	11.48	33.42	90.56	83.01
	Proposed Method	**6.19**	**11.49**	**3.25**	**5.82**	**7.24**	**3.94**	**6.19**	**7.54**	**3.77**
PS-II	Ensemble features [29]	6.99	11.83	5.83	19.18	42.71	32.59	5.45	6	3.6
	Hybrid features [25]	3.45	2.17	1.14	28.63	73.24	57.63	12.89	23.15	16.8
	Deep features [22]	18.12	30.70	23.84	11.12	19.38	11.49	4.82	4.81	2.05
	Steerable features [24]	22.94	81.47	67.06	28.41	89.70	71.35	27.14	81.99	63.12
	Proposed Method	**2.19**	**2.6**	**1.22**	**9.19**	**15.6**	**9.19**	**1.73**	**0.85**	**0.17**

- The performance of the S-MAD techniques indicate the best detection accuracy when trained and tested on the same data medium compared to the cross-medium in all four different experiments. The proposed method has indicated the best results when trained and tested with the same medium compared to the existing methods in all four experiments.
- Comparing the quantitative results before and after post-processing (from Experiment-1 and 2), the performance of the S-MAD techniques are degraded when trained and tested across the data medium. However, the performance of the MAD techniques did not degrade when trained and tested on the same data medium. These results indicated that the performance of the S-MAD algorithms are less affected by the post-processing if the algorithms are trained and tested using the same type of data medium. However, post-processing has an impact on the performance of S-MAD techniques only with cross data medium. Further, it is interesting to note that that proposed method has indicated the best performance compared to SOTA on both after and before post-processing data, including the cross-data medium.

TABLE 8. Quantitative performance of the proposed method on Experiment-3.

Training data	MAD algorithms	Testing Data								
		Digital			PS-I			PS-II		
		D-EER(%)	BPCER@APCER		D-EER(%)	BPCER@APCER		D-EER(%)	BPCER@APCER	
			5%	10%		5%	10%		5%	10%
Digital	Ensemble features [29]	0.18	0	0	50	97.56	93.48	36.18	87.3	78.73
	Hybrid features [25]	0.18	0	0	50	93.65	89.53	42.72	87.13	77.35
	Deep features [22]	0.2	0	0	47.10	89.46	77.28	25.54	55.91	45.96
	Steerable features [24]	3.27	1.54	0.63	49.45	96.53	84.78	29.00	80.44	66.89
	Proposed Method	**0**	**0**	**0**	**45.81**	**95.19**	**87.99**	**24.68**	**79.41**	**65.35**
PS-I	Ensemble features [29]	21.19	45.96	34.99	10.27	19.13	11.49	13.36	24.56	15.95
	Hybrid features [25]	15.27	36.53	24.52	18.54	51.11	34.99	25.72	63.46	50.25
	Deep features [22]	26.27	56.43	44.25	8.72	9.89	14.28	15.45	27.78	19.21
	Steerable features [24]	22.27	75.12	53.17	13.99	42.02	25.21	35.81	89.87	79.41
	Proposed Method	**8.74**	**18.35**	**8.74**	**6.56**	**9.19**	**4.63**	**6.14**	**7.37**	**3.94**
PS-II	Ensemble features [29]	12.72	24.35	14.92	18.18	39.1	30.18	4.72	4.8	3.14
	Hybrid features [25]	5.26	6.65	3.25	27.19	73.92	53	13.91	29.33	19.72
	Deep features [22]	22.81	45.79	36.70	13.64	28.81	18.36	6.54	7.89	4.28
	Steerable features [24]	24.91	81.30	66.03	33.09	82.33	71.35	28.27	74.78	60.89
	Proposed Method	**6.82**	**8.57**	**4.28**	**11.84**	**19.13**	**13.34**	**2.73**	**1.37**	**0.68**

TABLE 9. Quantitative performance of the proposed method on Experiment-4.

Training data	MAD algorithms	Testing Data								
		Digital			PS-I			PS-II		
		D-EER(%)	BPCER@APCER		D-EER(%)	BPCER@APCER		D-EER(%)	BPCER@APCER	
			5%	10%		5%	10%		5%	10%
Digital	Ensemble features [29]	0.18	0	0	40.8	95.54	86.96	37.16	88.16	80.27
	Hybrid features [25]	0.36	0	0	41.98	90.56	79.41	40.8	85.93	77.35
	Deep features [22]	**0**	**0**	**0**	40.14	74.85	63.51	35.04	85.46	58.73
	Steerable features [24]	3.09	1.54	0.34	39.59	80.55	77.29	31.05	82.50	72.21
	Proposed Method	**0**	**0**	**0**	**38.89**	**93.36**	**79.47**	**30.87**	**88.16**	**80.27**
PS-I	Ensemble features [29]	20.76	45.14	36.36	8.74	14.16	7.54	13.57	27.95	18.52
	Hybrid features [25]	12.84	29.84	16.29	16.3	48.37	30.36	24.22	59.34	44.59
	Deep features [22]	18.05	35.76	28.55	5.19	5.31	2.74	13.29	27.27	16.32
	Steerable features [24]	19.76	55.17	42.36	10.84	22.29	12.17	32.78	86.62	76.50
	Proposed Method	**7.18**	**10.29**	**4.13**	**4.28**	**3.77**	**2.15**	**7.14**	**8.41**	**5.48**
PS-II	Ensemble features [29]	8.19	13.37	6.17	17.48	42.13	31.9	6.17	7.54	4.14
	Hybrid features [25]	4.46	3.24	1.54	28.96	72.55	59.34	14.13	28.47	18.86
	Deep features [22]	15.12	24.50	20.98	10.10	18.35	10.12	6.19	7.29	3.43
	Steerable features [24]	21.13	75.54	57.28	30.50	86.44	72.55	26.22	83.36	60.72
	Proposed Method	**8.65**	**12.34**	**7.54**	**8.74**	**12.69**	**8.4**	**1.91**	**1.37**	**0.68**

- Based on the obtained results from Experiments-3 and 4, MAD techniques are trained on after post-processing and tested on before post-processing and vice versa. These two experiments will provide insights into the influence of detection accuracy on post-processing. Also, we evaluate the same in cross data medium experiments. As indicated in the Table 8 and 9, the MAD techniques has indicated less degradation when same data medium is used for training and testing. However, the detection performance is degraded when the cross-medium is used in training and testing. Thus, the post-processing of the morphed images indicates the influence in detection accuracy only across cross-medium.
- Overall, the proposed method has indicated the best performance across all four different experiments and thus indicated less influence to the post-processing data. For simplicity, we have shown the DET plots (see Figure 9) on Experiment-4 indicating the performance of the proposed method.

D. RESULTS AND DISCUSSION ON DB-III

In this section, we present the quantitative results of the proposed method with the existing methods on the age

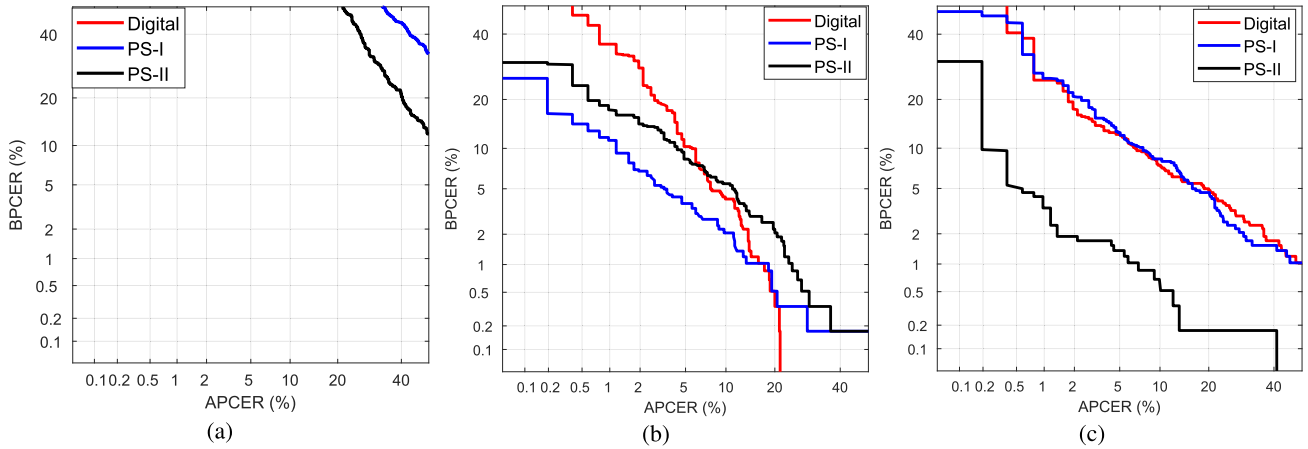

FIGURE 9. DET Curves showing the performance of the proposed method on Experiment-4 (a) Train on Digital (b) Train on PS-I (c) Train on PS-II.

TABLE 10. Experiment-I: Quantitative performance of the MAD techniques on MorphAge-I.

Algorithm	Development Set	Testing set			
	D-EER (%)	D-EER (%)	BPCER (%) @ APCER (%) =		
			1	5	10
Morphing factor (α) 0.3					
LBP-SVM [23]	28.14	35.11	84.4	68.8	56.8
BSIF-SVM [23]	31.82	37.59	98.8	90	73.2
HOG-SVM [28]	32.09	33.51	84.4	63.6	53.6
AlexNet-SVM [17]	4.38	2	7.2	3.2	0.8
Color Denoising [31]	1.63	3.65	5.2	0.4	0.4
Steerable features [24]	27.48	22.48	72.28	60.15	48.65
Deep features [22]	**0**	**0**	**0**	**0**	**0**
Ensemble features [29]	**0**	**0**	**0**	**0**	**0**
Hybrid features [25]	**0**	**0**	**0**	**0**	**0**
Proposed Method	**0**	**0**	**0**	**0**	**0**
Morphing factor (α) 0.5					
LBP-SVM [23]	27.82	33.76	75.2	59.2	57.2
BSIF-SVM [23]	31.82	36.9	98.8	89.21	73.6
HOG-SVM [28]	30.73	34.1	81.2	63.2	56.8
AlexNet-SVM [17]	3.18	2.01	4.12	0	0
Color Denoising [31]	1.63	1.21	7.6	0.4	0
Steerable features [24]	25.48	25.48	75.18	62.15	51.75
Deep features [22]	**0**	**0**	**0**	**0**	**0**
Ensemble features [29]	**0**	**0**	**0**	**0**	**0**
Hybrid features [25]	**0**	**0**	**0**	**0**	**0**
Proposed Method	**0**	**0**	**0**	**0**	**0**
Morphing factor (α) 0.7					
LBP-SVM [23]	28.86	34.92	88.4	66.8	57.2
BSIF-SVM [23]	31.9	37.98	98.8	88	73.2
HOG-SVM [28]	32.98	33.38	80	62.8	57.2
AlexNet-SVM [17]	5.08	2.78	5.6	2	0
Color Denoising [31]	2.75	2.43	13.2	2	0.4
Steerable features [24]	29.45	31.81	83.83	74.15	65.57
Deep features [22]	**0**	**0**	**0**	**0**	**0**
Ensemble features [29]	**0**	**0**	**0**	**0**	**0**
Hybrid features [25]	**0**	**0**	**0**	**0**	**0**
Proposed Method	**0**	**0**	**0**	**0**	**0**

TABLE 11. Experiment-I: Quantitative performance of the MAD techniques on MorphAge-II.

Algorithm	Development Set	Testing set			
	D-EER (%)	D-EER (%)	BPCER (%) @ APCER (%) =		
			1	5	10
Morphing factor (α) 0.3					
LBP-SVM [23]	30.64	29.21	61.24	48.83	44.96
BSIF-SVM [23]	33.35	39.17	58.91	51.16	48.83
HOG-SVM [28]	32.56	32.56	66.66	51.93	45.73
AlexNet-SVM [17]	4	5.49	7.75	4.65	4.65
Color Denoising [31]	3.15	1.7	3.1	0	0
Steerable features [24]	31.45	35.87	88.46	77.46	73.44
Deep features [22]	2.75	1.97	3.41	0	0
Ensemble features [29]	**0**	**0**	**0**	**0**	**0**
Hybrid features [25]	**0**	**0**	**0**	**0**	**0**
Proposed Method	**0**	**0**	**0**	**0**	**0**
Morphing factor (α) 0.5					
LBP-SVM [23]	28.71	32.39	68.99	48.06	41.08
BSIF-SVM [23]	32.65	39	63.56	51.16	48.83
HOG-SVM [28]	30.33	32.56	62.02	52.71	44.96
AlexNet-SVM [17]	2.92	3.78	6.2	3.87	3.11
Color Denoising [31]	3.77	0.75	1.55	0.77	0.77
Steerable features [24]	33.45	30.87	85.56	75.96	67.44
Deep features [22]	2.81	1.51	1.55	0	0
Ensemble features [29]	**0**	**0**	**0**	**0**	**0**
Hybrid features [25]	**0**	**0**	**0**	**0**	**0**
Proposed Method	**0**	**0**	**0**	**0**	**0**
Morphing factor (α) 0.7					
LBP-SVM [23]	29.33	27.03	58.91	51.98	45.73
BSIF-SVM [23]	34.7	33.07	58.91	51.16	48.06
HOG-SVM [28]	31.02	29.09	73.64	58.91	44.96
AlexNet-SVM [17]	3.15	5.5	11.62	5.42	4.65
Color Denoising [31]	3.15	0.75	3.1	0	0
Steerable features [24]	31.65	29.87	78.56	72.46	61.54
Deep features [22]	1.35	1.78	2.41	0	0
Ensemble features [29]	**0**	**0**	**0**	**0**	**0**
Hybrid features [25]	**0**	**0**	**0**	**0**	**0**
Proposed Method	**0**	**0**	**0**	**0**	**0**

variation datasets [32]. We have followed the same performance evaluation protocol that of [32] with the same images used for training and testing. Table 10, 11 and 12 presents the quantitative results of the proposed method together with the existing methods. Based on the obtained results following are the main observation:

TABLE 12. Experiment-II: Quantitative detection performance of MAD techniques on MorphAge-I v/s. MorphAge-II.

Algorithm	Development Set	Testing set			
	D-EER (%)	D-EER (%)	BPCER (%) @ APCER (%) =		
			1	5	10
Morphing factor (α) 0.3					
LBP-SVM [23]	28.14	34.19	92.24	65.89	47.28
BSIF-SVM [23]	31.82	44.13	100	98.44	84.49
HOG-SVM [28]	32.09	41.86	91.47	70.54	62.01
AlexNet-SVM [17]	4.38	3.03	8.52	3.10	2.32
Color Denoising [31]	1.63	2.27	1.55	0.45	0
Steerable features [24]	32.65	34.53	85.88	75.36	65.14
Deep features [22]	3.15	1.7	3.1	0	0
Ensemble features [29]	**0**	**0**	**0**	**0**	**0**
Hybrid features [25]	**0**	**0**	**0**	**0**	**0**
Proposed Method	**0**	**0**	**0**	**0**	**0**
Morphing factor (α) 0.5					
LBP-SVM [23]	27.82	33.29	86.04	66.66	48.06
BSIF-SVM [23]	31.82	45.42	100	96.89	84.49
HOG-SVM [28]	30.73	37.95	85.27	67.44	57.36
AlexNet-SVM [17]	3.18	0.94	3.10	0.77	0.39
Color Denoising [31]	1.63	1.59	0.7	0	0
Steerable features [24]	30.35	31.63	82.78	72.86	61.24
Deep features [22]	2.25	1.75	2.91	0	0
Ensemble features [29]	**0**	**0**	**0**	**0**	**0**
Hybrid features [25]	**0**	**0**	**0**	**0**	**0**
Proposed Method	**0**	**0**	**0**	**0**	**0**
Morphing factor (α) 0.7					
LBP-SVM [23]	28.86	32.24	93.20	65.89	49.61
BSIF-SVM [23]	31.90	37.33	100	96.89	84.49
HOG-SVM [28]	32.98	33.54	88.37	68.99	58.13
AlexNet-SVM [17]	5.08	2.27	6.97	3.87	0.77
Color Denoising [31]	2.75	2.46	3.10	0.40	0
Steerable features [24]	31.55	33.33	77.58	67.66	58.14
Deep features [22]	3.35	1.55	2.31	0	0
Ensemble features [29]	**0**	**0**	**0**	**0**	**0**
Hybrid features [25]	**0**	**0**	**0**	**0**	**0**
Proposed Method	**0**	**0**	**0**	**0**	**0**

- The morphing factor does not influence the performance of the proposed method used to generate the morphing images. It can also be observed that the ageing factor does not influence the performance of the proposed method.
- The detection performance of the proposed method is not influenced by the cross-age experiments as reported in Table 12. However, most of the existing methods has indicated degraded performance.
- In general, the proposed method indicates the outstanding detection performance in all three experiments that can be attributed to the complementary information that can be extracted using multi-modality. Figure 10 shows the distribution of the bona fide and morph scores from the proposed method on all three experiments with a morphing factor of 0.5. The obtained results indicate the clear separation of the bona fide and morph scores that shows the robustness of the proposed method to ageing.

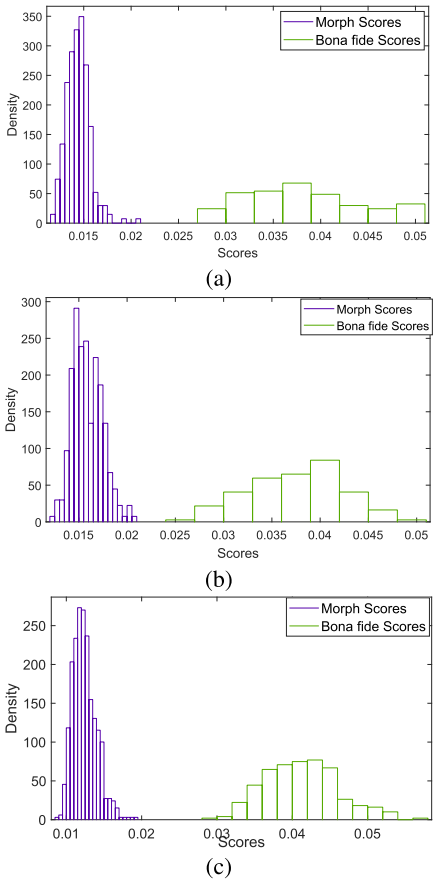

FIGURE 10. Score distribution showing the performance of the proposed method with Morphing Factor = 0.5 on DB-III (a) Experiment-I: MorphAge-I (b) Experiment-I: MorphAge-II (c) Experiment-II: MorphAge-I v/s. MorphAge-II.

E. EXECUTION TIME OF MAD ALGORITHMS

This section presents the discussion on the execution time for the individual MAD algorithms employed on three different databases in this work. The execution time is calculated by including the time to read a face image from storage, process it with face detection, pre-processing operation to have a face region of dimension 250 × 250 pixels, feature extraction and testing with a trained model to get the final decision. Table 13 shows executing time of 10 different MAD algorithms that are evaluated in this work for the single probe face image. All the MAD algorithms are evaluated on the windows machine with Intel(R) Xeon(R) CPU E5-2660 v3 processor with 256GB RAM and developed using MATLAB. It is important to note that none of these MAD algorithms is optimised to run fast except that the proposed method is implemented to extract features in parallel. As noted from Table 13 the execution time of the MAD algorithms increases with the complexity of the algorithms as some of the MAD techniques reported in Table 13 use multiple feature extraction and classification algorithms. Among the different MAD techniques, the proposed method shows the high execution time attributed to the use of multimodality. However, with professional code optimisation and sophisticated hardware, the proposed

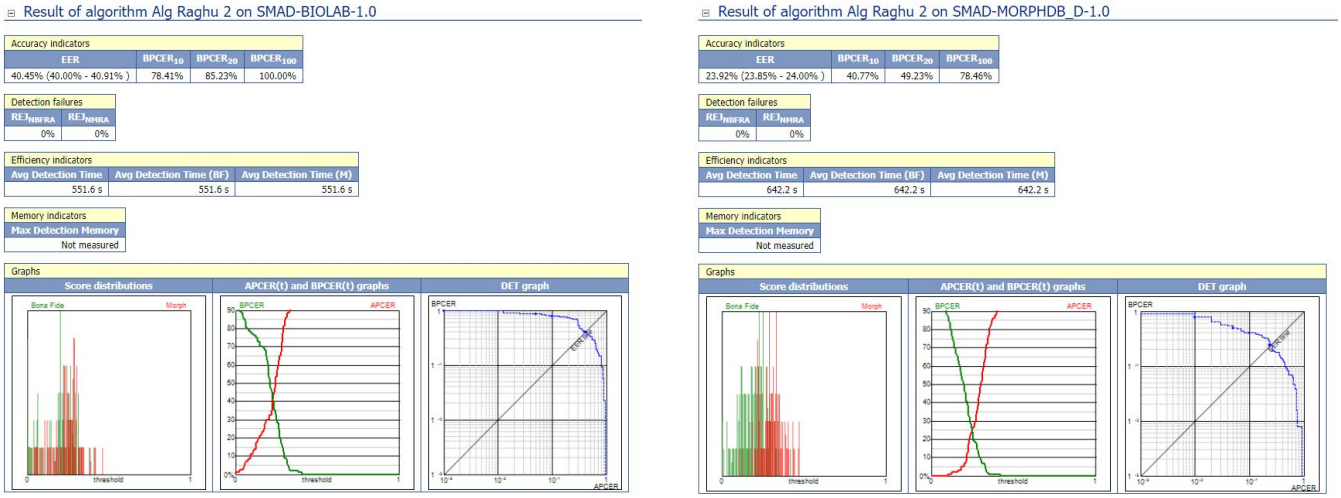

(a) Results on SMAD-BIOLAB-1.0 benchamrk

(b) Results on SMAD-MORPHDB_D-1.0 benchmark

FIGURE 11. Quantitative results from Bologna Online Evaluation Platform (BOEP).

TABLE 13. Execution time of MAD algorithms.

MAD Algorithms	Computation Time in seconds
LBP-SVM [23]	0.56
BSIF-SVM [23]	0.72
HOG-SVM [28]	0.52
AlexNet-SVM [17]	0.72
Color Denoising [31]	0.98
Steerable features [24]	0.85
Deep features [22]	1.24
Ensemble features [29]	2.45
Hybrid features [25]	2.12
Proposed Method	3.75

S-MAD method can be easily deployed in real-life experiments to achieve reliable detection accuracy.

IV. DISCUSSION

Based on the extensive experiments conducted, obtained results and the observations made above, the research questions formulated in Section I are answered below.

- **Q1**. Does the use of multimodality will improve the overall performance of S-MAD?
  - Based on the extensive experiments reported using three different datasets with varying characteristics (like morphing generation type, manual post-processing and ageing), the proposed method has consistently out-performed the existing S-MAD techniques. Thus, the proposed method has indicated the best performance in detecting the single image face morphing attacks.
- **Q2**. Does the proposed S-MAD algorithm can indicate superior performance irrespective of the morphing generation techniques (e.g. landmark and deep learning-based)?
  - Based on the results reported on DB-I in which the proposed method is evaluated on five different morph generation techniques. The proposed method shows the improved performance over existing S-MAD techniques on all five different types of morph generation.
- **Q3**. Does the proposed method indicates improved performance on the morphing data with ageing?
  - Based on the results obtained on DB-III, the proposed method has indicated an outstanding performance on all three experiments compared to the existing methods. Thus, the use of multimodality together with the proposed features extraction and classifications scheme has resulted in the robust S-MAD system for ageing variation.
- **Q4**. Does the manual post-processing to remove morphing artefacts in the morphed face image can degrade the performance of the proposed method?
  - Based on the obtained results on the DB-II, the manual post-processing of the morphed face images will impact the detection performance of both the proposed method and existing methods. The proposed method has indicated the best performance even with manual post-processing data.
- **Q5**. Does the proposed method can result in improved generalisability to an unknown source of morphing process when compared to existing methods?
  - Based on the extensive experiments, the proposed method has indicated the improved performance over existing state-of-the-art on all three databases. Thus, indicating the improved generalisability to an unknown source of morphing process

V. BENCHMARK RESULTS FROM BOLOGNA ONLINE EVALUATION PLATFORM (BOEP)

In this section, we present the quantitative results of the proposed method on the Bologna Online Evaluation Platform (BOEP) [1]. The proposed method is trained using the data from all three different mediums such as: digital, print-scan and print-scan compression. The training data is sampled from all three datasets used in this work that are

discussed in section III-A. Figure 11a and 11b shows the performance of the proposed method on BOEP benchmark with two different datasets such as: SMAD-BIOLAB-1.0 [11] and SMAD-MORPHDB_D-1.0 [12] respectively. For the detailed description of these datasets readers can refer to Bologna Online Evaluation Platform (BOEP) [1]. Based on the obtained results following can be noticed:

- The proposed method indicates the variation in the detection accuracy depending on the type of the dataset used for the testing.
- The proposed method indicates the performance with D-ERR = 23.92% on the SMAD-MORPHDB_D-1.0 [12] and D-EER = 40.45% on SMAD-BIOLAB-1.0 [11] dataset.
- The performance variation of the proposed method can be attributed to the variation in the data used for testing as well as for training. The degraded performance noted with SMAD-BIOLAB-1.0 [11] can be attributed to the nature of image manipulations in the dataset. SMAD-BIOLAB-1.0 dataset includes the face morphing images generated from manually generated landmarks and manually retouched.
- The obtained benchmarking results are similar to the cross dataset results reported in our experiments in Section III-B. These results justifies our finding on generalising to unknown morphing attacks are challenging especially in the S-MAD scenario.

VI. CONCLUSION

This work presented a new framework to detect face morphing attacks based on a single image. The proposed method will explore the multimodal regions from the face that include eyes, mouth, and nose processed independently using feature extraction and classification. In this work, we have used BSIF and LBP to extract both course and detailed texture features from the multimodal regions. The extracted features are classified independently using P-CRC and SRKDA, whose scores are combined at multiple levels to make the final decision. Extensive experiments are carried out on three different datasets to benchmark the proposed method's detection performance and the existing methods. Experimental evaluation protocols are designed to benchmark the detection performance on cross morph generation techniques, manual post-processing and ageing variation. The proposed method has indicated the best performance over existing methods on all three datasets with different performance evaluation protocols. The obtained results demonstrate the efficacy of the proposed framework for reliable single image-based morph attack detection.

REFERENCES

[1] *Bologna Online Evaluation Platform (BOEP)*. Accessed: Apr. 4, 2022. [Online]. Available: https://biolab.csr.unibo.it/fvcongoing/UI/Form/boep.aspx
[2] (2017). *Face Morph Using OpenCV*. Accessed: Apr. 10, 2017. [Online]. Available: https://learnopencv.com/face-morph-using-opencv-cpp-python/
[3] O. A. Abisoye and A. D. Mohammed, "Face morphing attack detection in the presence of post-processed image sources using neighborhood component analysis and decision tree classifier," in *Proc. 3rd Int. Conf. Inf. Commun. Technol. Appl. (ICTA)*, vol. 1350. Minna, Nigeria: Springer, Nov. 2020, p. 340.
[4] P. Aghdaie, B. Chaudhary, S. Soleymani, J. Dawson, and N. M. Nasrabadi, "Attention aware wavelet-based detection of morphed face images," in *Proc. IEEE Int. Joint Conf. Biometrics (IJCB)*, Aug. 2021, pp. 1–8.
[5] P. Aghdaie, B. Chaudhary, S. Soleymani, J. Dawson, and N. M. Nasrabadi, "Detection of morphed face images using discriminative wavelet sub-bands," 2021, *arXiv:2106.08565*.
[6] B. Yip, G. Bingham, K. Kempfert, J. Fabish, T. Kling, C. Chen, and Y. Wang, "Preliminary studies on a large face database," in *Proc. IEEE Int. Conf. Big Data (Big Data)*. IEEE, 2018, pp. 2572–2579.
[7] P. Burt and E. Adelson, "The Laplacian pyramid as a compact image code," *IEEE Trans. Commun.*, vol. 31, no. 4, pp. 532–540, Apr. 2003.
[8] N. Damer, N. Spiller, M. Fang, F. Boutros, F. Kirchbuchner, and A. Kuijper, "PW-MAD: Pixel-wise supervision for generalized face morphing attack detection," 2021, *arXiv:2108.10291*.
[9] L. Debiasi, C. Rathgeb, U. Scherhag, A. Uhl, and C. Busch, "PRNU variance analysis for morphed face image detection," in *Proc. IEEE 9th Int. Conf. Biometrics Theory, Appl. Syst. (BTAS)*, Oct. 2018, pp. 1–9.
[10] M. Ferrara, A. Franco, and D. Maltoni, "The magic passport," in *Proc. IEEE Int. Joint Conf. Biometrics*, Sep. 2014, pp. 1–7.
[11] M. Ferrara, A. Franco, and D. Maltoni, *Face Recognition Across the Imaging Spectrum, chapter On the Effects of Image Alterations on Face Recognition Accuracy*. Cham, Switzerland: Springer, 2016, pp. 195–222.
[12] M. Ferrara, A. Franco, and D. Maltoni, "Face demorphing," *IEEE Trans. Inf. Forensics Security*, vol. 13, no. 4, pp. 1008–1017, Apr. 2018.
[13] M. Ferrara, A. Franco, and D. Maltoni, "Decoupling texture blending and shape warping in face morphing," in *Proc. Int. Conf. Biometrics Special Interest Group (BIOSIG)*, Sep. 2019, pp. 1–5.
[14] W. T. Freeman and E. H. Adelson, "The design and use of steerable filters," *IEEE Trans. Pattern Anal. Mach. Intell.*, vol. 13, no. 9, pp. 891–906, Sep. 1991.
[15] *Information Technology Biometric Presentation Attack Detection—Part 3: Testing and Reporting*, Standard ISO/IEC JTC1 SC37 Biometrics. ISO/IEC 30107-3, International Organization for Standardization, 2017.
[16] A. Makrushin, T. Neubert, and J. Dittmann, "Humans Vs. algorithms: Assessment of security risks posed by facial morphing to identity verification at border control," in *Proc. 14th Int. Joint Conf. Comput. Vis., Imag. Comput. Graph. Theory Appl.*, 2019, pp. 513–520.
[17] M. Ferrara, A. Franco, and D. Maltoni, "Face morphing detection in the presence of printing/scanning and heterogeneous image sources," 2019, *arXiv:1901.08811*.
[18] M. Ngan, P. Grother, K. Hanaoka, and J. Kuo, "Face recognition vendor test (FRVT)—Part 4: MORPH-performance of automated face Morph detection," Nat. Inst. Technol. (NIST), Gaithersburg, MD, USA, Tech. Rep. NISTIR, 8292, 2021.
[19] P. J. Phillips, P. J. Flynn, T. Scruggs, K. W. Bowyer, J. Chang, K. Hoffman, J. Marques, J. Min, and W. Worek, "Overview of the face recognition grand challenge," in *Proc. IEEE Comput. Soc. Conf. Comput. Vis. Pattern Recognit. (CVPR)*, vol. 1, Jun. 2005, pp. 947–954.
[20] R. Raghavendra and C. Busch, "Novel image fusion scheme based on dependency measure for robust multispectral palmprint recognition," *Pattern Recognit.*, vol. 47, no. 6, pp. 2205–2221, Jun. 2014.
[21] R. Raghavendra, K. Raja, S. Venkatesh, and C. Busch, "Face morphing versus face averaging: Vulnerability and detection," in *Proc. IEEE Int. Joint Conf. Biometrics (IJCB)*, Oct. 2017, pp. 555–563.
[22] R. Raghavendra, K. B. Raja, S. Venkatesh, and C. Busch, "Transferable deep-CNN features for detecting digital and print-scanned morphed face images," in *Proc. IEEE Conf. Comput. Vis. Pattern Recognit. Workshops (CVPRW)*, Jul. 2017, pp. 1822–1830.
[23] R. Raghavendra, K. B. Raja, and C. Busch, "Detecting morphed face images," in *Proc. IEEE 8th Int. Conf. Biometrics Theory, Appl. Syst. (BTAS)*, Sep. 2016, pp. 1–8.
[24] R. Raghavendra, S. Venkatesh, K. Raja, and C. Busch, "Detecting face morphing attacks with collaborative representation of steerable features," in *Proc. IAPR Int. Conf. Comput. Vis. Image Process. (CVIP)*, 2018, pp. 1–7.
[25] R. Ramachandra, S. Venkatesh, K. Raja, and C. Busch, "Towards making morphing attack detection robust using hybrid scale-space colour texture features," in *Proc. IEEE 5th Int. Conf. Identity, Secur., Behav. Anal. (ISBA)*, Jan. 2019, pp. 1–7.

[26] K. Raja *et al.*, "Morphing attack detection-database, evaluation platform, and benchmarking," *IEEE Trans. Inf. Forensics Security*, vol. 16, pp. 4336–4351, 2021.
[27] U. Scherhag, A. Nautsch, C. Rathgeb, M. Gomez-Barrero, R. N. J. Veldhuis, L. Spreeuwers, M. Schils, D. Maltoni, P. Grother, S. Marcel, R. Breithaupt, R. Ramachandra, and C. Busch, "Biometric systems under morphing attacks: Assessment of morphing techniques and vulnerability reporting," in *Proc. Int. Conf. Biometrics Special Interest Group (BIOSIG)*, Sep. 2017, pp. 1–7.
[28] U. Scherhag, R. Raghavendra, K. B. Raja, M. Gomez-Barrero, C. Rathgeb, and C. Busch, "On the vulnerability of face recognition systems towards morphed face attacks," in *Proc. 5th Int. Workshop Biometrics Forensics (IWBF)*, Apr. 2017, pp. 1–6.
[29] S. Venkatesh, R. Ramachandra, K. Raja, and C. Busch, "Single image face morphing attack detection using ensemble of features," in *Proc. IEEE 23rd Int. Conf. Inf. Fusion (FUSION)*, Jul. 2020, pp. 1–5.
[30] S. Venkatesh, R. Ramachandra, K. Raja, L. Spreeuwers, R. Veldhuis, and C. Busch, "Detecting morphed face attacks using residual noise from deep multi-scale context aggregation network," in *Proc. IEEE Winter Conf. Appl. Comput. Vis. (WACV)*, Mar. 2020, pp. 1–8.
[31] S. Venkatesh, R. Ramachandra, K. Raja, L. Spreeuwers, R. Veldhuis, and C. Busch, "Morphed face detection based on deep color residual noise," in *Proc. 9th Int. Conf. Image Process. Theory, Tools Appl. (IPTA)*, Nov. 2019, pp. 1–8.
[32] S. Venkatesh, K. Raja, R. Ramachandra, and C. Busch, "On the influence of ageing on face morph attacks: Vulnerability and detection," in *Proc. IEEE Int. Joint Conf. Biometrics (IJCB)*, Sep. 2020, pp. 1–8.
[33] S. Venkatesh, R. Ramachandra, and K. Raja, "Face morphing of newborns can be threatening too : Preliminary study on vulnerability and detection," in *Proc. IEEE Int. Joint Conf. Biometrics (IJCB)*, Aug. 2021, pp. 1–8.
[34] S. Venkatesh, R. Ramachandra, K. Raja, and C. Busch, "Face morphing attack generation and detection: A comprehensive survey," *IEEE Trans. Technol. Soc.*, vol. 2, no. 3, pp. 128–145, 2021.
[35] S. Venkatesh, H. Zhang, R. Ramachandra, K. Raja, N. Damer, and C. Busch, "Can GAN generated morphs threaten face recognition systems equally as landmark based morphs?—Vulnerability and detection," in *Proc. 8th Int. Workshop Biometrics Forensics (IWBF)*, Apr. 2020, pp. 1–6.
[36] H. Zhang, S. Venkatesh, R. Ramachandra, K. Raja, N. Damer, and C. Busch, "MIPGAN—Generating strong and high quality morphing attacks using identity prior driven GAN," *IEEE Trans. Biometrics, Behav., Identity Sci.*, vol. 3, no. 3, pp. 365–383, Jul. 2021.

RAGHAVENDRA RAMACHANDRA (Senior Member, IEEE) received the Ph.D. degree in computer science and technology from the University of Mysore, Mysore India and Institute Telecom, and Telecom SudParis, Evry, France (carried out as a collaborative work), in 2010. He was a Researcher with the Istituto Italiano di Tecnologia, Genoa, Italy, where he worked with video surveillance and social signal processing. He is currently a Full Professor at the Institute of Information Security and Communication Technology (IIK), Norwegian University of Science and Technology (NTNU), Gjøvik, Norway. He is also working as a Research and Development Chief at MOBAI AS. He has authored several articles and is a reviewer for several international conferences and journals. He also holds several patents in biometric presentation attack detection and morphing attack detection. His main research interests include deep learning, machine learning, data fusion schemes, and image/video processing, with applications to biometrics, multimodal biometric fusion, human behavior analysis, and crowd behavior analysis. He has received several best paper awards. He has also been involved in various conference organizing and program committees and has served as an associate editor for various journals. He has participated (as a PI, a Co-PI or a Contributor) in several EU projects, IARPA USA, and other national projects. He is serving as an Editor for the ISO/IEC 24722 standards on multimodal biometrics and an Active Contributor for the ISO/IEC SC 37 standards on biometrics.

GUOQIANG LI (Member, IEEE) received the bachelor's degree from Jilin University, China, in 2005, the master's degree from the Harbin Institute of Technology, China, in 2007, and the Ph.D. degree in information security from the Norwegian University of Technology and Science (NTNU), Gjøvik, Norway, in 2016. He is currently working as a Senior Researcher at the Institute of Information Security and Communication Technology (IIK), NTNU. He also holds a post as a Chief Scientist at MOBAI AS, Norway. He has participated in several EU projects, such as FIDELITY Project, PIDaaS Project, and iMARS Project, and a couple of national projects. His research interests include related to fingerprint recognition, face recognition, biometric template protection, behavioral biometrics, and image processing.